


PAPER

[View Article Online](#)
[View Journal](#) | [View Issue](#)Cite this: *Catal. Sci. Technol.*, 2022, 12, 6838**Effect of SO₂ poisoning on undoped and doped Mn-based catalysts for selective catalytic reduction of NO_x**Javier Ruiz-Martínez, ^{*,a} Lieven E. Gevers,^a Linga R. Enakonda,^a Ameen Shahid^a and Fei Wen^b

In this work, the poisoning effect of SO₂ was investigated in binary MnTi and ternary MnCeTi mixed oxides for the NH₃-SCR reaction under conditions relevant for mobile applications. For the binary MnTi sample, catalytic activity increases up to 250 °C, and then drops due to the oxidation of ammonia to NO_x. The addition of Ce decreases the catalytic activity at 150 °C but widens the optimal operational temperature and reaches high conversion at 350 °C. Upon performing activity test with 100 ppm of SO₂ in the gas stream, catalytic activity drastically decreases in all catalyst samples. The shape of the deactivation curve and SO₂ concentrations at the outlet of the reactor suggest a strong adsorption and poisoning of SO₂ on all the catalysts. Although samples containing large amounts of Ce display a better SO₂ tolerance, this is insufficient to be considered for practical applications. Deactivated samples were investigated by a wide range of characterization tools. N₂ physisorption measurements reveal a drop in the surface area that could partially explain catalyst deactivation. TGA reveals the absence of (NH₄)₂SO₄ on the deactivated samples and suggests the formation of Mn and Ce sulfates on the catalyst surface. XPS results confirm the formation of MnSO₄ and also show a decrease in the Mn and Ce oxidation states. Analysis of the redox function by catalytic NO oxidation and H₂-TPR experiments shows a strong loss of redox function upon SO₂ deactivation, which could explain the decrease of NH₃-SCR catalytic activity. Upon unraveling the effect and cause of deactivation, a doping study was performed. As in the binary MnTi and ternary MnCeTi, catalytic activity strongly decreases upon the introduction of SO₂ in the gas stream. None of the dopants investigated was able to suppress SO₂ deactivation, which suggest that other dopants or strategies should be pursued to commercialize Mn-based catalysts for low-temperature applications.

Received 11th July 2022,
Accepted 28th September 2022

DOI: 10.1039/d2cy01151d

rsc.li/catalysis

1. Introduction

Selective catalytic reduction (SCR) with ammonia is one of the most promising technologies to abate nitric oxides (NO_x, which includes NO and NO₂) under lean-burning conditions encountered in mobile lean-burn engines and stationary applications.^{1–3} Currently, there is a search for more efficient SCR catalysts motivated by the ever-increasing demand of stringent global legislation for improving air quality.⁴ V₂O₅-WO₃/TiO₂ catalysts provide high NO_x removal efficiency (over 90%) at high gas-hourly space velocities (60 000–90 000 h^{−1})

and between 250 and 400 °C.^{5–8} Unfortunately, the emission of toxic V oxides during operation has restricted such catalysts for mobile applications. Cu-CHA zeolites (Cu-SSZ-13 and Cu-SAPO-34) have been revolutionary in SCR applications due to their high activity and broader operational temperature (200–450 °C).^{9–11} Still, great advances in engine technology have brought more efficient combustion engines and consequently lower exhaust temperatures, which makes NO_x more refractory to abate, even for Cu-zeolites. Due to this situation, low-temperature (below 200 °C) catalysts are required. In this field, Mn-based catalysts have exhibited optimal NH₃-SCR activity due to their strong redox functionality. Typically, Mn-oxide catalysts contain other metal oxides that serve as supports and modulate their catalytic properties. Although Mn-oxide catalysts have shown their superior performance at low-temperature NH₃-SCR, they are not commercialized in automotive applications. One of the main reasons is their strong intolerance to SO₂,^{12–15} which is due to the combustion of sulfur contaminants in

^a King Abdullah University of Science and Technology, KAUST Catalysis Center, Catalysis Nanomaterials and Spectroscopy (CNS), Thuwal 23955, Saudi Arabia. E-mail: javier.ruizmartinez@kaust.edu.sa

^b Umicore AG & Co. KG, Rodenbachener Chaussee 4, 63457 Hanau-Wolfgang, Germany

† Electronic supplementary information (ESI) available. See DOI: <https://doi.org/10.1039/d2cy01151d>



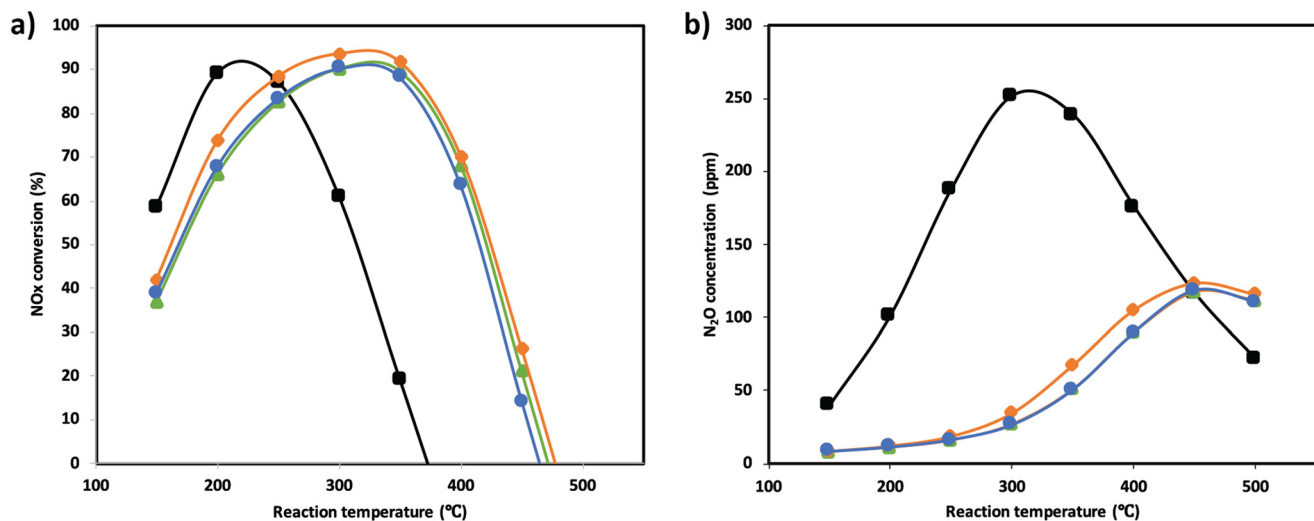


Fig. 1 NO_x conversion (a) and N₂O concentration (b) as a function of the reaction temperature for Mn_{0.35}Ce_{0.00}Ti_{0.65} (black), Mn_{0.37}Ce_{0.04}Ti_{0.59} (orange), Mn_{0.33}Ce_{0.07}Ti_{0.60} (green), and Mn_{0.30}Ce_{0.19}Ti_{0.51} (blue).

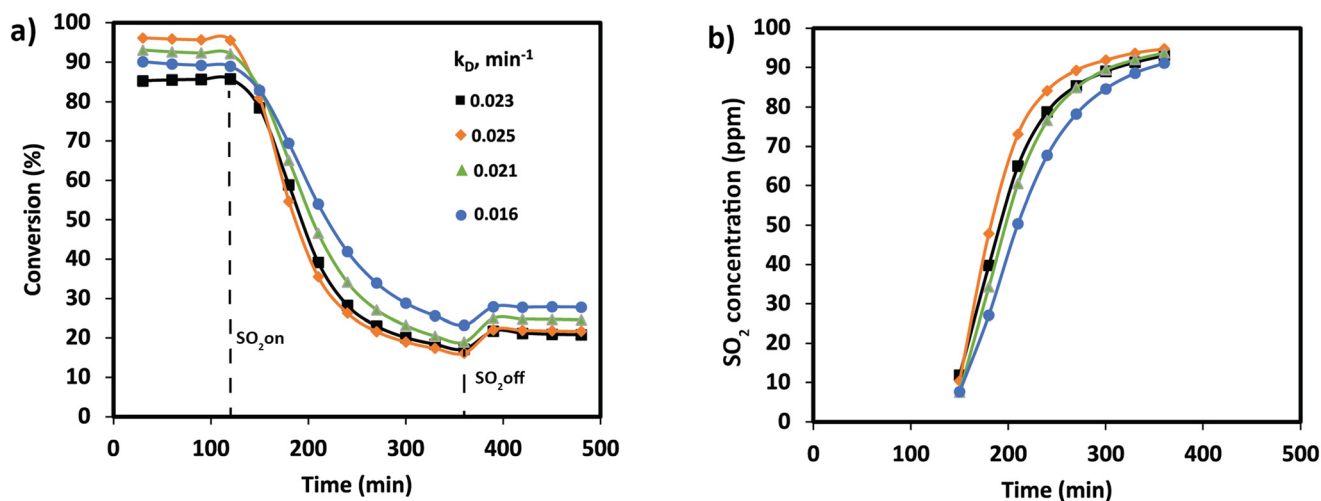


Fig. 2 a) Conversion plots and deactivation constants and b) SO₂ concentration at the outlet during the deactivation experiments performed at 250 °C for Mn_{0.35}Ce_{0.00}Ti_{0.65} (black), Mn_{0.37}Ce_{0.04}Ti_{0.59} (orange), Mn_{0.33}Ce_{0.07}Ti_{0.60} (green), and Mn_{0.30}Ce_{0.19}Ti_{0.51} (blue).

fuels and lubricants. Although the SO₂ concentration could be as low as a few ppm, those are sufficient to effectively poison Mn-oxide catalyst's active sites.

Several studies have discussed the detrimental effect of SO₂ on Mn-based catalysts and the deactivation effect has been explained by two main reasons. The first one is due to the reaction of SO₂ and NH₃ and H₂O to form (NH₄)₂SO₄ and NH₄HSO₄, which deposit on the catalyst surface and have a

high decomposition temperature (230 and 350 °C), respectively.^{16,17} The second one is related to the formation of metal sulfates that might modify or deactivate the active sites. Blik *et al.* investigated the SO₂ deactivation of MnO_x/Al₂O₃ catalysts by IR spectroscopy and found that the formation of MnSO₄ is the main source of deactivation.¹⁸ There are reports describing the regeneration of SO₂-poisoned catalysts can be efficient by water washing.¹⁹ Unfortunately, this approach is unfeasible for *in situ* catalyst regeneration in a real mobile application. To solve this deactivation process, catalyst formulations were modified with Fe,^{20–23} Co,^{24,25} Ni,^{26,27} W²⁸ and Sm^{29,30} to improve their tolerance to SO₂ and H₂O. For example, Wang *et al.* shown that Fe and Co co-doping reduces the adsorption of SO₂ on Mn–Ce/TiO₂ catalysts.²³ Sm-doped mixed oxide catalysts were shown to exhibit considerably enhanced catalytic activity and

Table 1 SO₂ uptake during deactivation experiments

Sample	SO ₂ uptake (μmol g ⁻¹)	SO ₂ uptake (μmol m ⁻²)
Mn _{0.35} Ce _{0.00} Ti _{0.65}	139	1.2
Mn _{0.37} Ce _{0.04} Ti _{0.59}	119	0.6
Mn _{0.33} Ce _{0.07} Ti _{0.60}	165	0.7
Mn _{0.30} Ce _{0.19} Ti _{0.51}	182	0.7



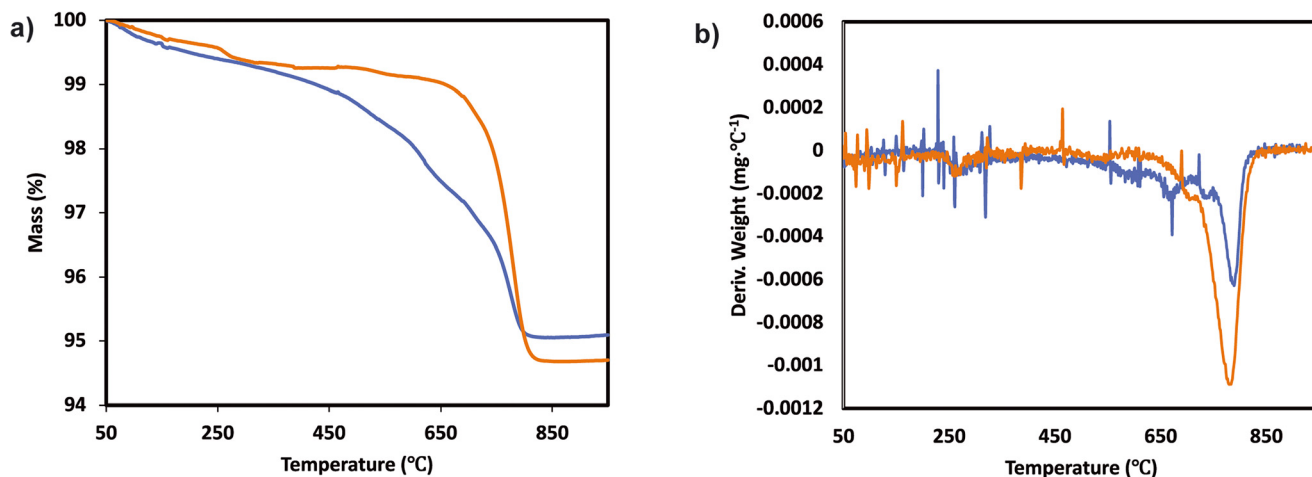


Fig. 3 a) TGA analysis and b) derivative thermogravimetric curves of the $\text{Mn}_{0.35}\text{Ce}_{0.00}\text{Ti}_{0.65}$ sample after normal NH_3 -SCR reaction (blue) and NH_3 -SCR reaction with SO_2 (yellow).

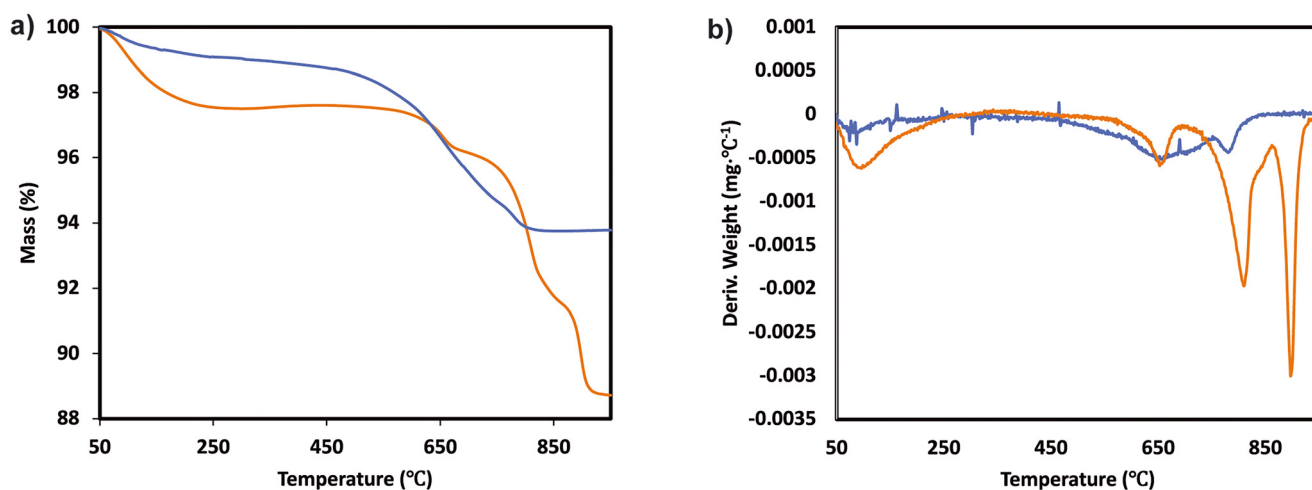


Fig. 4 a) TGA analysis and b) derivative thermogravimetric curves of the $\text{Mn}_{0.37}\text{Ce}_{0.04}\text{Ti}_{0.59}$ ternary system after normal NH_3 -SCR reaction (blue) and NH_3 -SCR reaction with SO_2 (yellow).

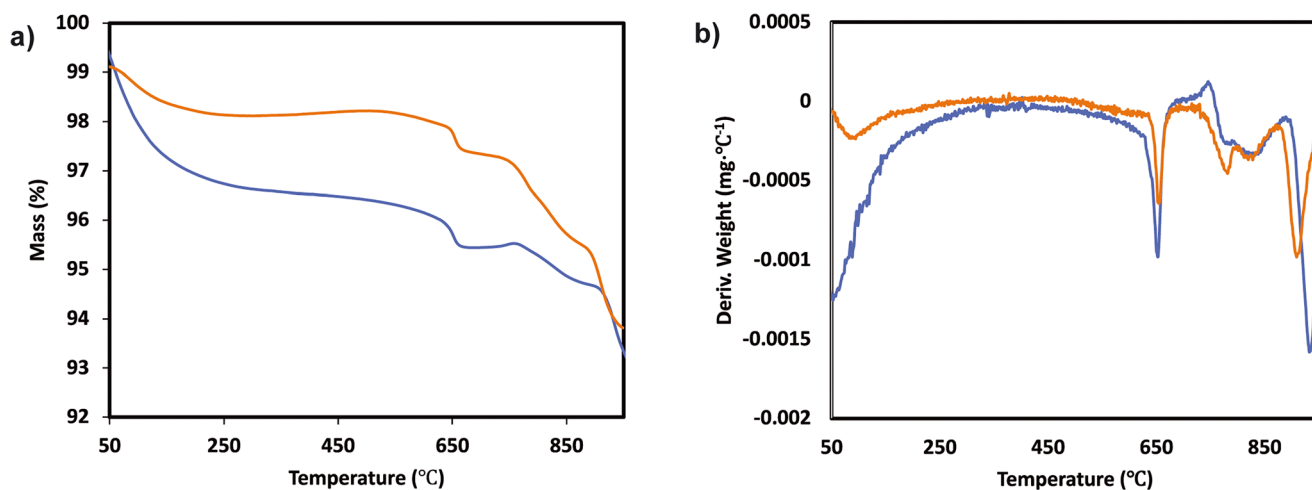


Fig. 5 a) TGA analysis and b) derivative thermogravimetric curves of the $\text{Mn}_{0.30}\text{Ce}_{0.19}\text{Ti}_{0.51}$ ternary system after normal NH_3 -SCR reaction (blue) and NH_3 -SCR reaction with SO_2 (yellow).



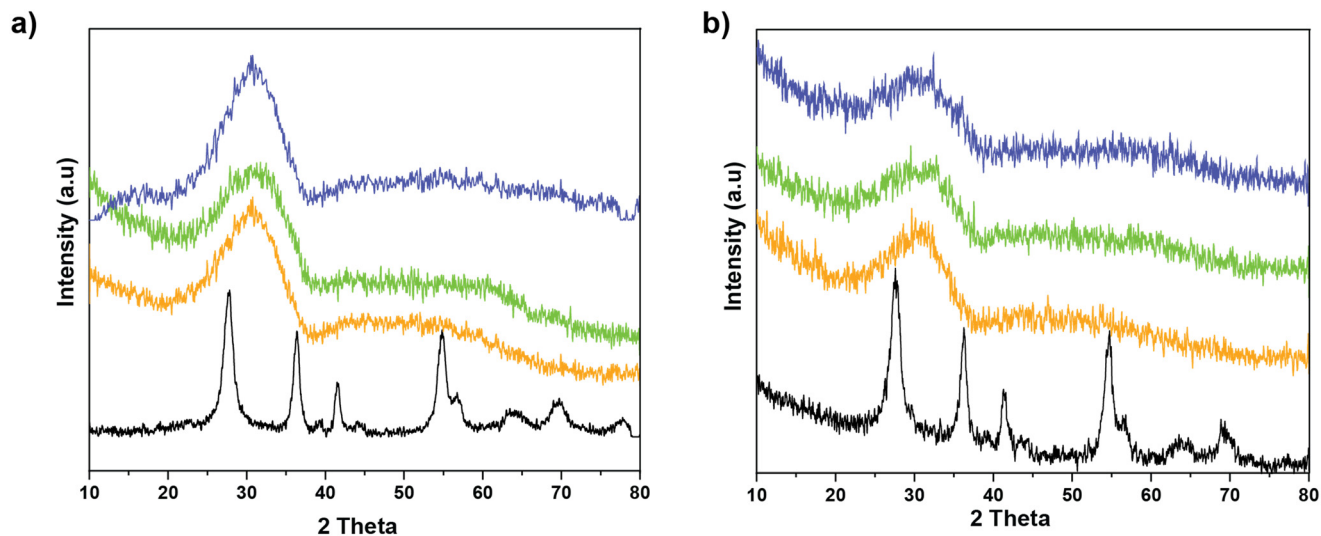


Fig. 6 X-ray diffraction patterns of the $\text{Mn}_{0.35}\text{Ce}_{0.00}\text{Ti}_{0.65}$ (black), $\text{Mn}_{0.37}\text{Ce}_{0.04}\text{Ti}_{0.59}$ (orange), $\text{Mn}_{0.33}\text{Ce}_{0.07}\text{Ti}_{0.60}$ (green), and $\text{Mn}_{0.30}\text{Ce}_{0.19}\text{Ti}_{0.51}$ (blue) samples: a) fresh and b) after SO_2 deactivation.

SO_2 tolerance. Sun *et al.*²⁹ found that the electron transfer from Sm^{2+} to Mn^{4+} restrained the electron transfer from SO_2 to Mn^{4+} , thereby suppressing the formation of SO_3 and sulfate species. Meng *et al.*³¹ found that a $\text{SmO}_x\text{-MnO}_x$ catalyst had an ideal SO_2 tolerance at low temperature, and they suggested that the incorporation of Sm could induce the formation of bulk-like sulfates on the Sm sites and weaken the influence of SO_2 on the Mn sites. However, the origin of the effect of Sm doping into the catalysts on the SO_2 tolerance is still unclear, and an in-depth study is still needed.

In this work, we aimed to understand the poisoning effect of SO_2 on a MnTi binary mixed oxide. Then, the role of Ce in catalyst deactivation was investigated in MnCeTi tertiary mixed oxides with different amounts of Ce. For this purpose, $\text{NH}_3\text{-SCR}$ reactions were performed by adding an amount of SO_2 equivalent to the total amount of S that a catalyst will be exposed in the exhaust of a real internal combustion engine after 200 000 km. The activity recovery was assessed by a regeneration step under high temperature and $\text{NH}_3\text{-SCR}$ conditions. These conditions were applied to simulate a theoretical regeneration in a real mobile application. After that, the catalysts were promoted by a wide range of metal dopants to evaluate the effect on poisoning and on catalyst regeneration.

2. Experimental

A series of individual, binary and ternary materials with different molar concentrations were prepared. Titanium(IV)

sulfate solution ($\text{Ti}(\text{SO}_4)_2$, Pfaltz & Bauer, 30% in H_2SO_4), cerium(III) nitrate hexahydrate ($\text{Ce}(\text{NO}_3)_3 \cdot 6\text{H}_2\text{O}$, Sigma-Aldrich, 99.999% trace metals basis), manganese(II) nitrate hydrate ($\text{Mn}(\text{NO}_3)_2 \cdot x\text{H}_2\text{O}$, Sigma-Aldrich, 99.999% trace metals basis), and ammonium hydroxide (NH_4OH , Alfa Aesar, ACS grade, 28.0–30.0%) were used as received, without further purification. The binary MnTi and ternary MnCeTi were prepared by a controlled co-precipitation method described in our previous publication.³² The method was designed to precipitate all metals at the same pH level to obtain a homogeneously well-mixed metal oxide system.

For the doping of the ternary MnCeTi catalysts, precipitation and impregnation methods were explored. In the precipitation method, a ternary MnCeTi was first suspended in an aqueous solution (50 mL). Then, 50 mL aqueous solution with the dopants were added slowly to the MnCeTi suspension, then the suspension was stirred for 30 min. After that, an aqueous ammonium hydroxide solution was added dropwise to the suspension under continuous stirring until a pH of 10.5 was reached. This was performed to precipitate all metal precursors on the catalyst surface. Afterwards, the suspension was stirred for another 1 h and then filtered. The solid product was washed with water 5–6 times, then dried in a hot air-oven overnight. For the impregnation method, 3 g of ternary MnCeTi sample were suspended in 50 mL of water. After 30 min of stirring, 50 mL of an aqueous solution of the dopant precursor were slowly added to the catalyst suspension. After stirring for 24 h, the suspension was evaporated and the solid was dried overnight. All catalysts were calcined at 500 °C for 6 h.

For the TG/DTA-MS analysis, 10–20 mg of sample was used. The samples were first kept at 30 °C for 30 min to stabilize the mass-loss signal. Then, the sample was heated with a ramp of 10 °C min^{-1} to 950 °C at 10 mL min^{-1} of air. The analysis of the gases was performed by mass

Table 2 Sulfur composition of the samples in the bulk and on the surface

Sample	Surface composition (mol%)	Bulk composition (mol%)
$\text{Mn}_{0.35}\text{Ce}_{0.00}\text{Ti}_{0.65}$	6.4	3
$\text{Mn}_{0.37}\text{Ce}_{0.04}\text{Ti}_{0.59}$	6.9	5.3
$\text{Mn}_{0.30}\text{Ce}_{0.19}\text{Ti}_{0.51}$	7.8	3.3



Table 3 Surface composition and chemistry of Mn and Ce species measured by XPS

Sample	Surface composition (at%)		Manganese				Cerium	
	Mn	Ce	MnO ₂	Mn ₂ O ₃	MnO	MnSO ₄	Ce(IV)	Ce(III)
Mn _{0.35} Ce _{0.00} Ti _{0.65}	15.2	0.0	17.9	66.1	16.0	0.0	0.0	0.0
Mn _{0.35} Ce _{0.00} Ti _{0.65} SO ₂	12.3	0.0	1.1	33.4	56.0	9.5	0.0	0.0
Mn _{0.37} Ce _{0.04} Ti _{0.59}	23.4	2.4	12.3	75.8	11.9	0.0	70.7	29.3
Mn _{0.37} Ce _{0.04} Ti _{0.59} SO ₂	18.2	2.7	19.6	18.8	53.6	8.0	36.3	63.7
Mn _{0.30} Ce _{0.19} Ti _{0.51}	14.5	6.3	20.6	27.3	42.3	9.7	66.2	33.8
Mn _{0.30} Ce _{0.19} Ti _{0.51} SO ₂	10.5	6.0	18.9	17.2	42.4	21.3	38.1	61.9

Table 4 Textural properties of the samples

Sample	BET surface area (m ² g ⁻¹)	Total pore volume (cm ³ g ⁻¹)	Pore size (nm)
Mn _{0.35} Ce _{0.00} Ti _{0.65}	117	0.45	14.0
Mn _{0.37} Ce _{0.04} Ti _{0.59}	200	0.53	9.5
Mn _{0.33} Ce _{0.07} Ti _{0.60}	222	0.63	10.0
Mn _{0.30} Ce _{0.19} Ti _{0.51}	243	0.86	12.5
Mn _{0.35} Ce _{0.00} Ti _{0.65} SO ₂	90	0.36	20.4
Mn _{0.37} Ce _{0.04} Ti _{0.59} SO ₂	142	0.51	13.1
Mn _{0.33} Ce _{0.07} Ti _{0.60} SO ₂	159	0.49	11.6
Mn _{0.30} Ce _{0.19} Ti _{0.51} SO ₂	147	0.44	11.2

spectrometry by following the signal from H₂O ($m/e = 18$), NO ($m/e = 30$), N₂O ($m/e = 44$) and SO₂ ($m/e = 48$).

X-ray diffraction patterns were obtained using a Bruker D8 Advance A25 diffractometer in the Bragg–Brentano geometry with a Cu K α , β radiation source operated at 40 kV and 40 mA. β radiation was filtered out with a Ni plate. The diffractograms were measured with a step size of 0.05° in the 2 θ range of 10–80°.

Nitrogen adsorption and desorption isotherms of the samples were measured at 77 K using a Micromeritics ASAP-2420 surface area and porosity analyzer instrument. The samples were previously evacuated at 300 °C for 3 hours. Specific surface areas and pore size distribution were calculated according to the multi-point Brunauer–Emmett–Teller (BET) and Barrett–Joyner–Halenda (BJH) methods,

respectively. From the adsorption data, total pore volumes were estimated at $P/P_0 = 0.99$. The elemental compositions (Mn, Ce, Ti) of the samples were determined using an inductively coupled plasma spectrometer (Model 8900, Agilent Technologies). The samples were dissolved in HF and HCl.

H₂-TPR experiments were performed on an Autochem 2950 instrument equipped with a thermal conductivity detector and a dry ice/isopropanol cold trap (−78 °C) to remove H₂O generated during the reduction. All catalysts (100 mg) were pretreated in a U-shaped quartz tubular microreactor in a flow of Ar at 250 °C for 2 h to yield a clean surface, and then cooled down to 40 °C temperature. Then, the temperature was raised from 40 to 1000 °C at a rate of 10 °C min^{−1} under a flow of 10 vol% H₂ (90 vol% Ar).

Temperature-programmed desorption of ammonia (NH₃-TPD) was used to determine the acidity of the fresh samples and samples deactivated by SO₂. The experiments were performed in a fixed bed quartz tube reactor. Prior to the measurement, the samples were first pretreated at 500 °C under a N₂ flow. The reactor was cooled down at 100 °C and the samples were saturated with 1050 ppm NH₃ for 30 min. The samples were flushed with N₂ for 30 min at room temperature, and then the temperature was increased to 500 °C at a rate of 10 K min^{−1}. The outlet gas composition (NH₃, NO, NO₂, N₂O) was monitored by using a MultiGas™ 2030 FTIR continuous gas analyzer.

For the XPS study, a Kratos Axis Ultra X-ray photoelectron spectrometer equipped with a monochromatic Al K α source was used to determine the surface composition and chemical states of the samples. The C 1s signal for adventitious carbon (284.8 eV) was used to calibrate the sample energy. The chemical states of manganese and cerium in the catalysts

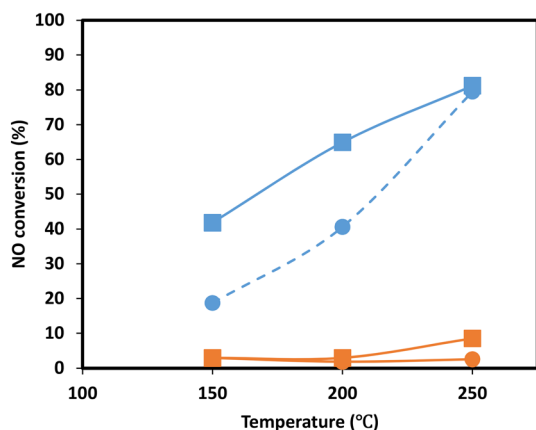


Fig. 7 NO oxidation experiments of Mn_{0.37}Ce_{0.04}Ti_{0.59} under dry (square) and wet (circle) conditions for the fresh sample (blue) and sample upon SO₂ deactivation (orange).



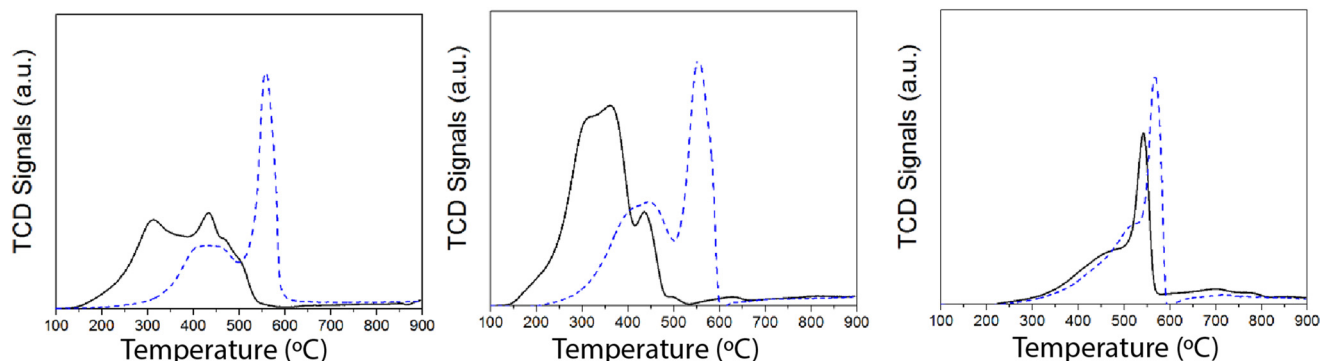


Fig. 8 H_2 -TPR results of S15, S24 and S28: fresh (solid line) and SO_2 deactivated (dashed line).

Table 5 NH_3 -SCR catalytic performance of sample $\text{Mn}_{0.37}\text{Ce}_{0.04}\text{Ti}_{0.59}$ and doped samples via precipitation (ppt) and impregnation (imp) methods

Sample	Conversion before deactivation (%)		Conversion after SO_2 deactivation (%)	Conversion after SO_2 regeneration (%)	
	150 °C	250 °C	250 °C	150 °C	250 °C
$\text{Mn}_{0.37}\text{Ce}_{0.04}\text{Ti}_{0.59}$	47	95	48	4	28
1% Sm/ $\text{Mn}_{0.37}\text{Ce}_{0.04}\text{Ti}_{0.59}$ (ppt)	53	98	35	2	24
1% V/ $\text{Mn}_{0.37}\text{Ce}_{0.04}\text{Ti}_{0.59}$ (ppt)	57	98	38	6	58
1% La/ $\text{Mn}_{0.37}\text{Ce}_{0.04}\text{Ti}_{0.59}$ (ppt)	68	98	47	6	34
1% Mo/ $\text{Mn}_{0.37}\text{Ce}_{0.04}\text{Ti}_{0.59}$ (imp)	45	96	28	4	52
1 wt% Eu/ $\text{Mn}_{0.37}\text{Ce}_{0.04}\text{Ti}_{0.59}$ (imp)	72	95	25	3	34

were determined by peak modeling in CasaXPS software. To model the Mn 2p_{3/2} peaks of the catalysts, pure MnO, Mn₂O₃, and MnO₂ samples were used as references. Manganese(IV) oxide (99.997% – metals basis) was acquired from Alfa Aesar (Fisher US), manganese(III) oxide (99.9% – trace metals basis) was acquired from Sigma Aldrich, and manganese(II) oxide (99.99% – trace metal basis) was acquired from Acros Organics (VWR). The fitting parameter data (FWHM and peak positions) obtained from the peak modeling of the standard samples were used for the calculation of the chemical state of manganese in our catalysts. More details about the fitting procedure and measurements can be obtained in our previous publication.³²

The catalytic activity measurements of the catalysts in the NH_3 -SCR reaction were carried out in a fixed bed quartz tube reactor loaded with 0.5 ml of sample (PID Eng&Tech). Before loading, the catalysts were pressed into pellets, crushed and sieved to obtain a fraction between 500 and 710 μm . The application-relevant catalyst particle size, space velocity and gas composition were applied. The inlet NO_x composition contained no NO_2 to avoid higher conversions coming from the “fast SCR” mechanism when this gas is present. The total flow rate was maintained at 1000 ml min⁻¹, and the reaction condition corresponds to a GHSV of 120 000 hr⁻¹. The flow rate of gases was controlled using Bronkhorst mass flow controllers. A controlled evaporation and mixing (CEM) system from Bronkhorst was used for evaporation to achieve the target steam content in the gas feed before entering the reactor. The inlet gas stream contained 450 ppm NO, 500 ppm NH_3 , 5% O₂, 5% H₂O and N₂ balance. A MultiGas™

2030 FTIR continuous gas analyzer was used to analyze the inlet and outlet gas compositions (NO, NO₂, NH_3 , N₂O). The catalytic tests were performed in the temperature range of 150–500 °C (with an interval of 50 °C) at ambient pressure. NO conversion and N₂O selectivities were calculated under steady-state conditions. The SCR activity (NO conversion) and N₂ selectivity are calculated as follows:

$$\text{NO conversion (\%)} = \frac{[\text{NO}]_{\text{in}} - [\text{NO}]_{\text{out}}}{[\text{NO}]_{\text{in}}} \times 100 \quad (1)$$

$$\text{N}_2\text{O selectivity (\%)} = \frac{2[\text{N}_2\text{O}]_{\text{out}}}{[\text{NO}_x]_{\text{in}} + [\text{NH}_3]_{\text{in}} - [\text{NO}_x]_{\text{out}} - [\text{NH}_3]_{\text{out}}} \times 100 \quad (2)$$

where $[\text{NH}_3]_{\text{in}}$, $[\text{NO}_x]_{\text{in}}$, $[\text{NH}_3]_{\text{out}}$, $[\text{NO}_x]_{\text{out}}$, and $[\text{N}_2\text{O}]_{\text{out}}$ are the concentrations of NH_3 and NO_x (including NO and NO₂) at the inlet and those at the outlet.

The NO oxidation reaction was performed in the same fashion as the NH_3 -SCR. In this case, 250 ppm of NO and 5% O₂ were fed to the reactor and balanced with N₂. In the experiments under wet conditions, 5% of vapor H₂O was included in the inlet gas stream.

3. Results

Activity measurements

NO_x conversion of the MnTi binary and MnCeTi ternary mixed oxides as a function of the reaction temperature is presented in Fig. 1. The data at 150 °C were determined to be free of external and internal mass transport limitations (more



details in the ESI†). In general, conversion increases until reaching a maximum, and then decreases with the reaction temperature. NH_3 conversion (ESI† Fig. S1) follows the same trend as NO_x conversion, but monotonically increases when the conversion drops. This mismatch in conversions is related to the undesired combustion of ammonia, which leads to the formation of additional NO_x in the gas stream. The binary MnTi catalyst is more active at low temperatures but lacks N_2 selectivity, showing a high concentration of N_2O at the outlet (see Fig. 1b). The addition of Ce has several effects on catalytic performance. First, low-temperature activity decreases suggesting that Mn species are less active due to the interaction with Ce, as we previously reported.³² Second, the addition of Ce widens the operational window, as was also reported previously,³ and finally promotes N_2 selectivity.

In order to understand the effect of SO_2 poisoning, experiments were performed where NO_x conversion was measured before and during SO_2 poisoning under NH_3 -SCR conditions. Fig. 2 shows the NH_3 -SCR conversion at 250 °C before and during SO_2 deactivation. When 100 ppm SO_2 is introduced in the stream, the conversion of all samples drastically decreased from $\approx 90\%$ to $\approx 20\%$ in 4 hours. Interestingly, the sample with the largest amount of Ce ($\text{Mn}_{0.30}\text{Ce}_{0.19}\text{Ti}_{0.51}$) displays a better sulfur tolerance. The S-type shape of the deactivation curves suggest that SO_2 is adsorbing strongly on the catalyst surface and deactivating the catalyst bed from the inlet to the outlet. Deactivation rates were consistently compared using second-order deactivation kinetics by applying the equation $da/dt = -k_D \cdot a^2$ where a is the normalized NO_x activity. Deactivation rate constants, in Fig. 2a, are more pronounced for the binary MnTi catalyst and the samples with a small amount of Ce ($\text{Mn}_{0.37}\text{Ce}_{0.04}\text{Ti}_{0.59}$). Then, deactivation constants drop when the amount of Ce increases, suggesting a lessening of deactivation with increasing Ce content. After removal of SO_2 from the feed gas, NO_x conversion is marginally recovered indicating that SO_2 deactivation is mostly irreversible.

SO_2 uptakes were calculated by monitoring the SO_2 concentration at the reactor outlet in Fig. 2b. Clearly, the drop in NO_x conversion is strongly related to the SO_2 uptake. The results show that all catalysts are adsorbing all SO_2 at the first stage of the experiment. Then, the SO_2 concentration is monotonically increasing until almost reaching the inlet concentration. SO_2 uptakes, in Table 1, show an increase in the uptake for MnCeTi ternary catalysts with higher Ce loading. To rule out the effect of the surface area on the SO_2 uptake, a surface normalization was applied. After such normalization, the results show a nearly constant SO_2 adsorption in the MnCeTi ternary systems and therefore an independency from the amount of Ce. In the case of the binary MnTi, the SO_2 uptake normalized by the surface area shows a twofold increase with respect to the Ce-containing samples. Our previous study showed that the surface of the binary MnTi samples is enriched with Mn,³² which would suggest that sulfur prefers Mn to either Ti or Ce.

In order to understand if there are sulfates formed and their chemistry, thermogravimetric analysis (TGA) was performed with the samples before and after SO_2 deactivation. The chemistry of the sulfate species was inferred by comparing the results with the TGA analysis results of pure $(\text{NH}_4)_2\text{SO}_4$, TiOSO_4 , MnSO_4 , and $\text{Ce}(\text{SO}_4)_2$. These results are included in the ESI† Fig. S2. The MnTi binary sample, in Fig. 3, shows a continuous decrease in mass loss after the normal NH_3 -SCR reaction, which could be related to the removal of species adsorbed after the reaction. In the NH_3 -SCR reaction with SO_2 , there is a lack of mass loss at around 400 °C for the SO_2 deactivated sample, which indicates that $(\text{NH}_4)_2\text{SO}_4$ is not present in the deactivated material. In contrast, there is a remarkable increase in the weight loss at around 780 °C, which is a temperature slightly lower than the decomposition temperature of MnSO_4 (see ESI†). Combined mass spectrometry measurements (in ESI† Fig. S3a) show an evolution of SO_2 coming out of the sample, suggesting the decomposition of a metal sulfate. We hypothesized that the weight loss is due to the decomposition of MnSO_4 and the fact that the decomposition temperature is slightly lower than that of pure bulk sulfates could be due to the fact that the sulfates might be finely dispersed on the catalyst surface. The existence of TiOSO_4 is discarded due to the lack of weight loss and SO_2 evolution at the decomposition temperature of such species.

The TGA analysis of the ternary $\text{Mn}_{0.37}\text{Ce}_{0.04}\text{Ti}_{0.59}$ and $\text{Mn}_{0.30}\text{Ce}_{0.19}\text{Ti}_{0.51}$ samples is shown in Fig. 4 and 5. The samples without deactivation show a slight mass loss around 800 °C with an SO_2 evolution, suggesting that there are some sulfates formed during the catalyst synthesis due the use of TiOSO_4 as a titanium precursor. All samples have also mass loss around 650 °C, which could be related to the decomposition of TiOSO_4 . However, this cannot be confirmed as there is no evolution of SO_3 in the mass spectrometer. Measuring SO_3 is quite challenging due to its highly reactive nature. Upon SO_2 deactivation, there are several decomposition events at around 800 °C, which could be ascribed to the formation of both Ce and Mn sulfates. The existence of sulfates is corroborated by the evolution of SO_2 during the TGA experiments.

To understand the structural changes occurring upon SO_2 deactivation, the crystalline structure of the samples before and after deactivation was investigated by X-ray diffraction (XRD). The results, in Fig. 6, show that the MnCe binary oxide show reflections of rutile TiO_2 , with no appearance of MnO_x phases. In the case of the MnCeTi ternary systems, the diffraction patterns lack any reflection indicating the amorphous nature of the samples. After SO_2 deactivation, the diffraction patterns resemble the fresh counterparts. The lack of additional crystalline phases indicates that the metal sulfates have an amorphous nature, most likely due to the formation of the sulfates solely on the catalyst surface.

To further investigate the location of the sulfur species on the catalysts, the bulk and surface composition of sulfur was investigated by ICP and XPS, respectively. Table 2 shows the



sulfur composition in mol%. Clearly, all the samples show a sulfur enrichment on the catalyst surface compared to the total bulk composition, in line with the hypothesis that sulfur species are created more preferentially on the catalyst surface.

Experiments to understand the acidity of the samples upon SO₂ deactivation were performed by temperature-programmed desorption of ammonia (NH₃-TPD). The temperature-programmed evolution of the binary Mn_{0.35}-Ce_{0.00}Ti_{0.65} sample is plotted in ESI† Fig. S4. The amount of NH₃ desorbed is more than double after SO₂ deactivation (see ESI† Table S1), which reflect the formation of new acid sites. This insight has also been reported previously and indicates the acidic nature of the new sulfate species formed on the surface.^{33–35} Additional information about the reactivity of oxygen species on the catalyst could be extracted from the evolution of N₂O during NH₃-TPD. Less N₂O is formed at higher temperature after SO₂ deactivation, which points to the loss of active oxygen during deactivation.

To gain more insight into the effect of SO₂, the chemistry of Mn and Ce was investigated by XPS. Oxidation states of Mn were rigorously fitted from a set of Gaussian-Lorentzian components per oxidation state, due to the multiplet splitting between the unpaired electrons in Mn 2+, 3+ and 4+. The set of components of the discrete oxidation states were obtained from measurements of pure MnSO₄, MnO, Mn₂O₃ and MnO₂ oxides and the results were compared with previously reported measurements.³⁶ The Mn 2p spectra of the reference samples and catalysts (fresh and SO₂ deactivated) are plotted in ESI† Fig. S5 and S6. Table 3 shows the surface composition and chemistry of Mn and Ce on selected samples. After SO₂ deactivation, Mn surface composition decreases whereas Ce remains nearly constant. The Mn (2p_{3/2}) spectra show an overall change in the composition of the samples to more reduced Mn species. Although Mn₂O₃ is dominant in the fresh samples, MnO is the most predominant species upon SO₂ deactivation. Additionally, a substantial amount of MnSO₄ is formed. Overall, around 60% of Mn⁴⁺ and Mn³⁺ gets reduced to Mn²⁺. Ce (3d) spectra show an increase in the concentration of Ce³⁺ upon deactivation (see also ESI† Fig. S7), which could be explained by the oxidation of SO₂ to SO₄²⁻ and the reduction of Ce⁴⁺ to Ce³⁺ with subsequent formation of sulfates.³⁷

The N₂ physisorption results, in Table 4, show a surface area of the MnTi binary sample of 117 m² g⁻¹. After the addition of Ce, there is an increase in the surface area and total pore volume, mostly related to the formation of an amorphous mixed-oxide phase. The samples after SO₂ deactivation show a drop in the specific surface area. In the case of the binary MnTi, 23% of the specific surface area is lost after deactivation. For the samples with Ce, the loss in the specific surface area increases with the amount of Ce (28, 29 and 40% for Mn_{0.33}Ce_{0.07}Ti_{0.60}, Mn_{0.37}Ce_{0.04}Ti_{0.59} and Mn_{0.30}Ce_{0.19}Ti_{0.51}, respectively). Other authors have also observed a decrease in the surface area upon SO₂ deactivation on Mn-based catalysts,^{18,38,39} mostly due to the

formation of surface sulphate species. Indeed, this loss in the surface area has a direct impact on catalyst deactivation. However, in our study, it can only explain catalyst deactivation to a limited extent. Therefore, this is not the main deactivation mechanism.

To gain more insight into the effect of SO₂ poisoning on catalytic performance, NO oxidation to NO₂ of the Mn_{0.37}-Ce_{0.04}Ti_{0.59} ternary sample was performed before and after SO₂ deactivation. This is a model reaction to investigate the behavior of the catalyst redox function, which is strongly related to its NH₃-SCR performance at low temperatures. Additionally, NO oxidation plays a key role in the fast SCR reaction, which is believed to be ten times faster than the standard reaction of NO with NH₃.^{40,41} As the NH₃-SCR reaction is performed under the presence of H₂O, the experiments were performed under dry and wet conditions. The results, in Fig. 7, show a clear drop in NO oxidation upon SO₂ deactivation in the range of temperatures investigated, suggesting that the redox function is drastically affected upon deactivation as it was also observed during the evolution of N₂O in the NH₃-TPD experiments. Several authors have also observed similar effects on CeO₂-MnO_x⁴² and MnO_x/TiO₂ (ref. 43) catalysts and postulate that the reason is the formation of Mn sulfates.

Since the redox function seems to be strongly affected after SO₂ deactivation, additional insights were obtained by temperature-programmed reduction (TPR) experiments with H₂. The H₂-TPR results of the samples (fresh and after SO₂ deactivation) are shown in Fig. 8. Overall, we ascribe the reduction of the H₂ consumption peak at 200–450 °C to the reduction of Mn⁴⁺ and Mn³⁺ to Mn²⁺.^{44,45} Upon SO₂ deactivation, there is a decrease in the H₂ consumed at those temperatures, most likely due to the overall reduction in the Mn oxidation state, as suggested by the XPS results. Additionally, H₂ consumption is shifted to higher temperatures, which could be rationalized as a consequence of the interaction of sulfate species with Mn. The strong H₂ consumption at 550–600 °C is related to the reduction of Mn and Ce sulfates.^{33,34,46}

Overall, our results shows that catalyst deactivation is mainly due to the formation of metal sulfates, most likely Mn and Ce sulfates. These metal sulfates are decreasing the oxidation states of Mn and Ce, which have a strong impact on the redox function of such metals. Additionally, SO₂ deactivation decreases the catalysts' total specific surface area, but this is not the main deactivation mechanism.

In order to improve the catalytic properties of the samples upon deactivation, a thorough doping study was performed. Catalytic performances of the selected samples (fresh and upon SO₂) and NH₃-SCR regeneration at 500 °C for 30 min are shown in Table 5. On the selected metal-doped catalysts, relatively high NH₃-SCR activities were obtained with the samples doped with Sm, V, La and Eu. Upon catalytic reaction with 100 ppm of SO₂, the NH₃-SCR activity was drastically decreased for both the undoped and doped samples. Therefore, the dopant seems to be ineffective in



avoiding catalyst deactivation under the investigated conditions.

To recover the catalyst activity, the samples were treated at 500 °C in 20% oxygen, as these conditions could be applied in a real exhaust of a combustion engine. The results show that in some samples, such conditions are even more detrimental, decreasing the catalyst activity upon SO₂ uptake. As exceptions, samples doped with V and Mo display an almost twofold increase in catalytic activity at 250 °C. As described in the literature, V and Mo are acidic metals and could inhibit the adsorption of SO₂ to some extent.⁴⁷ Unfortunately, activity at 150 °C is still poor, indicating that the addition of such metals is not sufficient to avoid the formation of Mn and Ce sulfates and therefore the loss of redox function. We hypothesized that the high activities at 250 °C are due to V and Mo themselves, which are active metals for NH₃-SCR and are not that drastically affected by SO₂ deactivation. However, such metals are not sufficiently active at low temperatures. Our results are contradicting other previously reported data, for example summarized elsewhere,³ where dopants improve sulfur tolerance. While reviewing those studies, one can see that most of them were performed at lower space velocities and/or in the absence of steam, which is not representative of a real application.

4. Conclusions

In this work, the poisoning effect of SO₂ was investigated in binary MnTi and ternary MnCeTi mixed oxides for the NH₃-SCR reaction under conditions relevant for mobile applications. Upon performing activity test with 100 ppm of SO₂ in the gas stream, the catalytic activity drastically decreases in all catalyst samples. The shape of the deactivation curve and SO₂ concentrations out of the reactor suggest a strong adsorption and poisoning of SO₂ on all the catalysts. Although samples containing large amounts of Ce display a better SO₂ tolerance, this is insufficient to be considered for realistic practical applications. Spent samples were investigated by a wide range of characterization tools. N₂ physisorption measurements reveal a drop in the surface area that could partially explain catalyst deactivation. TGA reveals the absence of (NH₄)₂SO₄ on the deactivated samples and suggests the formation of Mn and Ce sulfates on the catalyst surface. XPS results confirm the formation of MnSO₄ and also show a decrease in the Mn and Ce oxidation states. Analysis of the redox function by catalytic NO oxidation and H₂-TPR experiments shows a strong loss of redox function upon SO₂ deactivation, which could explain the decrease in NH₃-SCR catalytic activity. Upon unraveling the effect and cause of deactivation, the catalysts were modified by doping with a wide range of metals. As in the binary MnTi and ternary MnCeTi, catalytic activity strongly decreases upon the introduction of SO₂ in the gas stream. None of the dopants investigated was able to suppress SO₂ deactivation nor regenerate catalyst activity at low temperatures, which suggest that other dopants or strategies should be pursued to

commercialize Mn-based catalysts for low-temperature applications.

Conflicts of interest

The authors declare no competing interest.

Acknowledgements

The authors thank the financial support from Umicore N.V. (award number RGC/3/3291-01). The research was supported by the resources and facilities provided by the King Abdullah University of Science and Technology. The authors also acknowledge the KAUST Imaging and Characterization Core Lab. Lutz Ruwisch (Umicore) is kindly acknowledged for fruitful discussion.

References

- 1 J. L. Sorrels, Selective Catalytic Reduction. U.S. Environmental Protection Agency. <https://www.epa.gov/economic-and-cost-analysis-air-pollution-regulations/chapter-2-selective-catalytic-reduction>.
- 2 R. Zhang, N. Liu, Z. Lei and B. Chen, Selective Transformation of Various Nitrogen-Containing Exhaust Gases toward N₂ over Zeolite Catalysts, *Chem. Rev.*, 2016, **116**(6), 3658–3721.
- 3 L. Han, S. Cai, M. Gao, J. Y. Hasegawa, P. Wang, J. Zhang, L. Shi and D. Zhang, Selective Catalytic Reduction of NO_x with NH₃ by Using Novel Catalysts: State of the Art and Future Prospects, *Chem. Rev.*, 2019, **119**(19), 10916–10976.
- 4 T. V. Johnson, Diesel emission control in review, *SAE Int. J. Fuels Lubr.*, 2009, **1**(1), 68–81.
- 5 J. Chen and R. Yang, Role of WO₃ in mixed V₂O₅-WO₃/TiO₂ catalysts for selective catalytic reduction of nitric oxide with ammonia, *Appl. Catal., A*, 1992, **80**(1), 135–148.
- 6 T. Xu, X. Wu, Y. Gao, Q. Lin, J. Hu and D. Weng, Comparative study on sulfur poisoning of V₂O₅-Sb₂O₃/TiO₂ and V₂O₅-WO₃/TiO₂ monolithic catalysts for low-temperature NH₃-SCR, *Catal. Commun.*, 2017, **93**, 33–36.
- 7 X. Tian, Y. Xiao, P. Zhou, W. Zhang and X. Luo, Investigation on performance of V₂O₅-WO₃-TiO₂-cordierite catalyst modified with Cu, Mn and Ce for urea-SCR of NO, *Mater. Res. Innovations*, 2014, **18**(sup2), 202–206.
- 8 Z. Lian, Y. Li, W. Shan and H. He, Recent Progress on Improving Low-Temperature Activity of Vanadia-Based Catalysts for the Selective Catalytic Reduction of NO_x with Ammonia, *Catalysts*, 2020, **10**(12), 1421.
- 9 D. W. Fickel and R. F. Lobo, Copper coordination in Cu-SSZ-13 and Cu-SSZ-16 investigated by variable-temperature XRD, *J. Phys. Chem. C*, 2010, **114**(3), 1633–1640.
- 10 J. Girard, G. Cavataio, R. Snow and C. Lambert, Combined Fe-Cu SCR systems with optimized ammonia to NO_x ratio for diesel NO_x control, *SAE Int. J. Fuels Lubr.*, 2009, **1**(1), 603–610.
- 11 J. H. Kwak, R. G. Tonkyn, D. H. Kim, J. Szanyi and C. H. Peden, Excellent activity and selectivity of Cu-SSZ-13 in the



- selective catalytic reduction of NO_x with NH₃, *J. Catal.*, 2010, **275**(2), 187–190.
- 12 B. Jiang, Y. Liu and Z. Wu, Low-temperature selective catalytic reduction of NO on MnO_x/TiO₂ prepared by different methods, *J. Hazard. Mater.*, 2009, **162**(2), 1249–1254.
 - 13 S. Deng, T. Meng, B. Xu, F. Gao, Y. Ding, L. Yu and Y. Fan, Advanced MnO_x/TiO₂ Catalyst with Preferentially Exposed Anatase {001} Facet for Low-Temperature SCR of NO, *ACS Catal.*, 2016, **6**(9), 5807–5815.
 - 14 E. Park, M. Kim, H. Jung, S. Chin and J. Jurng, Effect of Sulfur on Mn/Ti Catalysts Prepared Using Chemical Vapor Condensation (CVC) for Low-Temperature NO Reduction, *ACS Catal.*, 2013, **3**(7), 1518–1525.
 - 15 S. Yu, Y. Lu, Y. Cao, J. Wang, B. Sun, F. Gao, C. Tang and L. Dong, Composite catalytic systems: A strategy for developing the low temperature NH₃-SCR catalysts with satisfactory SO₂ and H₂O tolerance, *Catal. Today*, 2019, **327**, 235–245.
 - 16 I. S. Nam, J. W. Eldridge and J. R. Kittrell, Deactivation of a vanadia-alumina catalyst for nitric oxide reduction by ammonia, *Ind. Eng. Chem. Prod. Res. Dev.*, 1986, **25**(2), 192–197.
 - 17 Q. Wang, J. Zhou, J. Zhang, H. Zhu, Y. Feng and J. Jin, Effect of ceria doping on catalytic activity and SO₂ resistance of MnO_x/TiO₂ catalysts for selective catalytic reduction of NO with NH₃ at low temperature, *Aerosol Air Qual. Res.*, 2020, **20**, 477–488.
 - 18 W. Sjoerd Kijlstra, M. Biervliet, E. K. Poels and A. Blik, Deactivation by SO₂ of MnO_x/Al₂O₃ catalysts used for the selective catalytic reduction of NO with NH₃ at low temperatures, *Appl. Catal., B*, 1998, **16**(4), 327–337.
 - 19 Z. Sheng, Y. Hu, J. Xue, X. Wang and W. Liao, SO₂ poisoning and regeneration of Mn-Ce/TiO₂ catalyst for low temperature NO_x reduction with NH₃, *J. Rare Earths*, 2012, **30**(7), 676–682.
 - 20 S. Wu, X. Yao, L. Zhang, Y. Cao, W. Zou, L. Li, K. Ma, C. Tang, F. Gao and L. Dong, Improved low temperature NH₃-SCR performance of FeMnTiO_x mixed oxide with CTAB-assisted synthesis, *Chem. Commun.*, 2015, **51**(16), 3470–3473.
 - 21 F. Liu, H. He, Y. Ding and C. Zhang, Effect of manganese substitution on the structure and activity of iron titanate catalyst for the selective catalytic reduction of NO with NH₃, *Appl. Catal., B*, 2009, **93**(1), 194–204.
 - 22 B. Q. Jiang, Z. B. Wu, Y. Liu, S. C. Lee and W. K. Ho, DRIFT Study of the SO₂ Effect on Low-Temperature SCR Reaction over Fe–Mn/TiO₂, *J. Phys. Chem. C*, 2010, **114**(11), 4961–4965.
 - 23 F. Wang, B. Shen, S. Zhu and Z. Wang, Promotion of Fe and Co doped Mn-Ce/TiO₂ catalysts for low temperature NH₃-SCR with SO₂ tolerance, *Fuel*, 2019, **249**, 54–60.
 - 24 H. Hu, S. Cai, H. Li, L. Huang, L. Shi and D. Zhang, Mechanistic Aspects of deNO_x Processing over TiO₂ Supported Co–Mn Oxide Catalysts: Structure–Activity Relationships and In Situ DRIFTS Analysis, *ACS Catal.*, 2015, **5**(10), 6069–6077.
 - 25 L. Huang, X. Hu, S. Yuan, H. Li, T. Yan, L. Shi and D. Zhang, Photocatalytic preparation of nanostructured MnO₂-(Co₃O₄)/TiO₂ hybrids: The formation mechanism and catalytic application in SCR deNO_x reaction, *Appl. Catal., B*, 2017, **203**, 778–788.
 - 26 J. Liu, X. Li, R. Li, Q. Zhao, J. Ke, H. N. Xiao, L. Wang, S. Liu, M. O. Tadè and S. Wang, Facile synthesis of tube-shaped Mn–Ni–Ti solid solution and preferable Langmuir–Hinshelwood mechanism for selective catalytic reduction of NO_x by NH₃, *Appl. Catal., A*, 2018, **549**, 289–301.
 - 27 L. Chen, R. Li, Z. Li, F. Yuan, X. Niu and Y. Zhu, Effect of Ni doping in NixMn1–xTi10 (x = 0.1–0.5) on activity and SO₂ resistance for NH₃-SCR of NO studied with in situ DRIFTS, *Catal. Sci. Technol.*, 2017, **7**(15), 3243–3257.
 - 28 X. Wang, X. Li, Q. Zhao, W. Sun, M. Tade and S. Liu, Improved activity of W-modified MnO_x–TiO₂ catalysts for the selective catalytic reduction of NO with NH₃, *Chem. Eng. J.*, 2016, **288**, 216–222.
 - 29 C. Sun, H. Liu, W. Chen, D. Chen, S. Yu, A. Liu, L. Dong and S. Feng, Insights into the Sm/Zr co-doping effects on N₂ selectivity and SO₂ resistance of a MnO_x–TiO₂ catalyst for the NH₃-SCR reaction, *Chem. Eng. J.*, 2018, **347**, 27–40.
 - 30 B. Wang, M. Wang, L. Han, Y. Hou, W. Bao, C. Zhang, G. Feng, L. Chang, Z. Huang and J. Wang, Improved Activity and SO₂ Resistance by Sm-Modulated Redox of MnCeSmTiO_x Mesoporous Amorphous Oxides for Low-Temperature NH₃-SCR of NO, *ACS Catal.*, 2020, **10**(16), 9034–9045.
 - 31 D. Meng, W. Zhan, Y. Guo, Y. Guo, L. Wang and G. Lu, A Highly Effective Catalyst of Sm–MnO_x for the NH₃-SCR of NO_x at Low Temperature: Promotional Role of Sm and Its Catalytic Performance, *ACS Catal.*, 2015, **5**(10), 5973–5983.
 - 32 L. E. Gevers, L. R. Enakonda, A. Shahid, S. Ould-Chikh, C. I. Q. Silva, P. P. Paalanen, A. Aguilar-Tapia, J.-L. Hazemann, M. N. Hedhili, F. Wen and J. Ruiz-Martínez, Unraveling the structure and role of Mn and Ce for NO_x reduction in application-relevant catalysts, *Nat. Commun.*, 2022, **13**(1), 2960.
 - 33 L. Zhang, L. Li, Y. Cao, X. Yao, C. Ge, F. Gao, Y. Deng, C. Tang and L. Dong, Getting insight into the influence of SO₂ on TiO₂/CeO₂ for the selective catalytic reduction of NO by NH₃, *Appl. Catal., B*, 2015, **165**, 589–598.
 - 34 M. Waqif, P. Bazin, O. Saur, J. C. Lavalley, G. Blanchard and O. Touret, Study of ceria sulfation, *Appl. Catal., B*, 1997, **11**(2), 193–205.
 - 35 J. Li, C. Zhang, Q. Li, T. Gao, S. Yu, P. Tan, Q. Fang and G. Chen, Promoting mechanism of SO₂ resistance performance by anatase TiO₂ {001} facets on Mn–Ce/TiO₂ catalysts during NH₃-SCR reaction, *Chem. Eng. Sci.*, 2022, **251**, 117438.
 - 36 M. C. Biesinger, B. P. Payne, A. P. Grosvenor, L. W. M. Lau, A. R. Gerson and R. S. C. Smart, Resolving surface chemical states in XPS analysis of first row transition metals, oxides and hydroxides: Cr, Mn, Fe, Co and Ni, *Appl. Surf. Sci.*, 2011, **257**(7), 2717–2730.
 - 37 R. M. Ferrizz, R. J. Gorte and J. M. Vohs, TPD and XPS Investigation of the Interaction of SO₂ with Model Ceria Catalysts, *Catal. Lett.*, 2002, **82**(1), 123–129.



- 38 B. Jiang, B. Deng, Z. Zhang, Z. Wu, X. Tang, S. Yao and H. Lu, Effect of Zr Addition on the Low-Temperature SCR Activity and SO₂ Tolerance of Fe-Mn/Ti Catalysts, *J. Phys. Chem. C*, 2014, **118**(27), 14866–14875.
- 39 J. Liu, R.-T. Guo, M.-Y. Li, P. Sun, S.-M. Liu, W.-G. Pan, S.-W. Liu and X. Sun, Enhancement of the SO₂ resistance of Mn/TiO₂ SCR catalyst by Eu modification: A mechanism study, *Fuel*, 2018, **223**, 385–393.
- 40 M. Koebel, M. Elsener and G. Madia, Reaction Pathways in the Selective Catalytic Reduction Process with NO and NO₂ at Low Temperatures, *Ind. Eng. Chem. Res.*, 2001, **40**(1), 52–59.
- 41 G. Madia, M. Koebel, M. Elsener and A. Wokaun, The Effect of an Oxidation Precatalyst on the NO_x Reduction by Ammonia SCR, *Ind. Eng. Chem. Res.*, 2002, **41**(15), 3512–3517.
- 42 F. Lin, Y. He, Z. Wang, Q. Ma, R. Whiddon, Y. Zhu and J. Liu, Catalytic oxidation of NO by O₂ over CeO₂-MnO_x: SO₂ poisoning mechanism, *RSC Adv.*, 2016, **6**(37), 31422–31430.
- 43 N. Tang, Y. Liu, H. Wang and Z. Wu, Mechanism Study of NO Catalytic Oxidation over MnO_x/TiO₂ Catalysts, *J. Phys. Chem. C*, 2011, **115**(16), 8214–8220.
- 44 F. Arena, T. Torre, C. Raimondo and A. Parmaliana, Structure and redox properties of bulk and supported manganese oxide catalysts, *Phys. Chem. Chem. Phys.*, 2001, **3**(10), 1911–1917.
- 45 X. Wu, Q. Liang, D. Weng, J. Fan and R. Ran, Synthesis of CeO₂-MnO_x mixed oxides and catalytic performance under oxygen-rich condition, *Catal. Today*, 2007, **126**(3), 430–435.
- 46 S. Yang, Y. Guo, H. Chang, L. Ma, Y. Peng, Z. Qu, N. Yan, C. Wang and J. Li, Novel effect of SO₂ on the SCR reaction over CeO₂: Mechanism and significance, *Appl. Catal., B*, 2013, **136–137**, 19–28.
- 47 D. W. Kwon, K. H. Park and S. C. Hong, Enhancement of SCR activity and SO₂ resistance on VO_x/TiO₂ catalyst by addition of molybdenum, *Chem. Eng. J.*, 2016, **284**, 315–324.

